CHEMISTRY OF MATERIALS

Article

pubs.acs.org/cm

Sodium-Induced Reordering of Atomic Stacks in Black Phosphorus

Yingchun Cheng,[†,§] Yihan Zhu,[∥] Yu Han,[∥] Zhongyuan Liu,[⊥] Bingchao Yang,[⊥] Anmin Nie,[*,‡,§] Wei Huang,[*,†] Reza Shahbazian-Yassar,[*,§] and Farzad Mashayek[*,§]

[†]Key Laboratory of Flexible Electronics (KLOFE) and Institute of Advanced Materials (IAM), Jiangsu National Synergetic Innovation Center for Advanced Materials (SICAM), Nanjing Tech University (NanjingTech), 30 South Puzhu Road, Nanjing 211816, China

[‡]Shanghai University Materials Genome Institute and Shanghai Materials Genome Institute, Shanghai University, Shanghai 200444, China

[§]Mechanical and Industrial Engineering Department, University of Illinois at Chicago, Chicago, Illinois 60607, United States

[∥]Advanced Membranes and Porous Materials Center, Physical Sciences and Engineering Division, King Abdullah University of Science and Technology, Thuwal 23955-6900, Saudi Arabia

[⊥]State Key Laboratory of Metastable Materials Science and Technology, Yanshan University, Qinhuangdao 066004, China

Supporting Information

ABSTRACT: While theoretical simulations predict contradictory results about how the intercalation of foreign metal atoms affects the order of atomic layers in black phosphorus (BP), no direct experimental visualization work has yet clarified this ambiguity. By in situ electrochemical sodiation of BP inside a high-resolution transmission electron microscope and first-principles calculations, we found that sodium intercalation induces a relative glide of $^1/_2$ ⟨010⟩ {001}, resulting in reordering of atomic stacks from AB to AC in BP. The observed local amorphization in our experiments is triggered by lattice constraints. We predict that intercalation of sodium or other metal atoms introduces n-type carriers in BP. This potentially opens a new field for two-dimensional electronics based on BP.

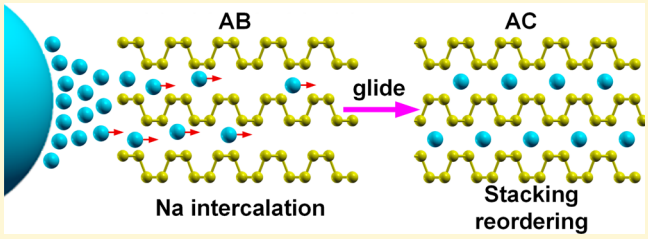

INTRODUCTION

Similar to graphite and MoS_2, black phosphorus (BP) is a layered material in which the individual layers are stacked in AB order by van der Waals interactions (Figure 1). Recently, multilayer phosphorene was fabricated by a mechanical exfoliation method and used in field-effect transistors (FETs).[1] The phosphorene-based FETs show extremely high charge-carrier mobilities of up to ~1000 $cm^2\ V^{-1}\ s^{-1}$. BP has raised a lot of attention due to its electronic properties.[1] One method to tune the properties of BP is to change the number of layers, which allows the band gap to be tuned from 0.3 to 2.0 eV.[2] Strain[3,4] and electric field[5,6] can also be used to modulate the electronic nature of BP. These property changes include semiconductor to Dirac semimetal, direct band gap to indirect band gap, and normal insulator to topological insulator transitions.

It has also been reported that the stacking order plays a significant role in the electronic properties of layered compounds, such as graphite[7] and MoS_2.[8,9] In lithium−graphite intercalation compounds, the graphene layers are in AA stacking order,[10,11] which implies that intercalation of foreign atoms is an effective way to change the stacking order. For bilayer phosphorene, the stacking order has been predicted to play a significant role in the power conversion efficiency of film solar cells,[12] in which AA, AB, and AC stacking orders have been discussed. Phosphorene has been predicted to have high diffusion anisotropy for lithium or sodium diffusion,[13,14] and this was recently verified experimentally.[15] Theoretically, it has been predicted by first-principles calculations that the stacking order of bulk BP will change from AB to AA upon lithium or sodium intercalation,[16] while another work predicted that lithium-intercalated BP will be superconducting and that the stacking order will change from AB to AC.[17] Such a contradiction should be clarified, and experimental and theoretical investigations are needed to gain a comprehensive view of the atomic structure evolution during intercalation of foreign atoms in BP.

In this work, we focus on the initial process of structure evolution for sodiation in bulk BP. We conducted a detailed investigation using high-resolution transmission electron microscopy (HRTEM) and observed the transition from AB to AC stacking order after sodium intercalation in bulk BP. By using first-principles calculations, we confirmed that the stacking order in bulk BP changes from AB to AC rather than to AA. We also noticed amorphization of BP besides the stacking ordering change after sodium intercalation in experi-

Received: November 28, 2016
Revised: January 11, 2017
Published: January 12, 2017

DOI: 10.1021/acs.chemmater.6b05052
Chem. Mater. 2017, 29, 1350−1356

ments. On the basis of simulations, we attribute such amorphization to the constraint of the lattice of bulk BP. Moreover, intercalation of sodium or other metal atoms in BP will induce electron doping, which has potential electronic applications.

RESULTS AND DISCUSSION

Figure 1a–d shows bulk BP in four different stacking orders: AA, AB, AC, and AD. The top views of the AA/AB and AC/AD stacking orders are identical, while the side views of AA/AC and AB/AD stacking orders appear to be the same. If the upper layer of AB stacking in BP shifts along the [100]/[010] direction by 50%, the structure is transformed to AA/AC stacking. If the upper layer of AB stacking shifts along both [100] and [010] by 50%, the AD stacking order is formed. From the side views, one can find that BPs with AC and AD stacking orders have more space than BPs with AA or AB stacking order, which suggests that AC or AD layering is preferable when ions intercalate between the layers.

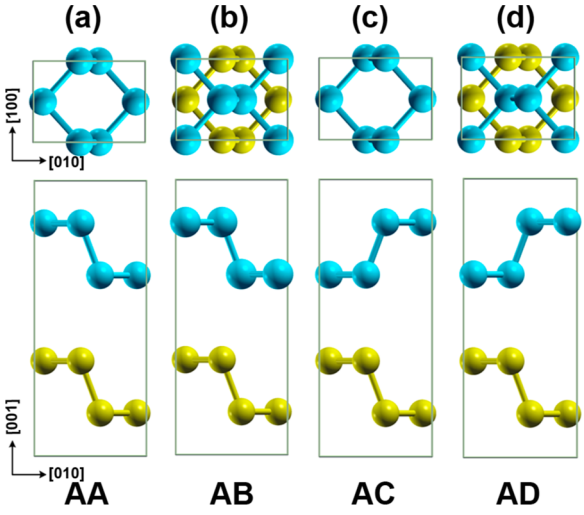

Figure 1. Top and side views of bulk BP for (a) AA, (b) AB, (c) AC, and (d) AD stacking order. Both blue and yellow balls represent phosphorus atoms. Two different colors are used to distinguish different layers for the eyes.

Figure 2a–c shows atomic high-angle annular dark-field (HAADF) images of pristine BP in different zone axes. The *d* spacings of two vertical lattice planes in Figure 2a were measured to be 5.27 and 4.36 Å, matching well with that of (002) and (010), respectively, of the orthorhombic BP structure (JCPDS no. 09-0020, space group *Bmab* (No. 64)). The other two atomic HAADF images (Figure 2b,c) were determined to be taken at the [010] and [001] zone axes. The corresponding atomic models, displayed in Figure 2d–f, clearly exhibit the atomic structure of the pristine BP sample. The consistent atomic HAADF observation firmly proves that the pristine BP sample used in this work has the AB stacking sequence.

Here we used in situ TEM to study the structure evolution of bulk BP during the sodiation process. Figure 3a shows a typical TEM image of partially sodiated BP. It can be observed that many dark contrast stripes with a specific orientation formed in the initial stage of the sodiation process in BP. The sodium element was detected inside the dark stripes by electron energy loss spectroscopy (EELS), as shown in Figure 3b. We can clearly see the peak centered at 31 eV that belongs to the sodium L edge. A selected-area electron diffraction (SAED) pattern was taken from the domain marked S_1 in Figure 3a together with some sodiation stripes (Figure 3c). According to the analysis of the SAED pattern, the BP was determined to be along the [001] projection and the orientation of the sodiation stripes is along the (020) planes. We can conclude that the sodium initially prefers to diffuse along the [100] direction of BP, which has been thoroughly discussed in our previous work.[15] We also found that the intensity of the {110} spots is much lower than that of the {020} spots in this SAED pattern.

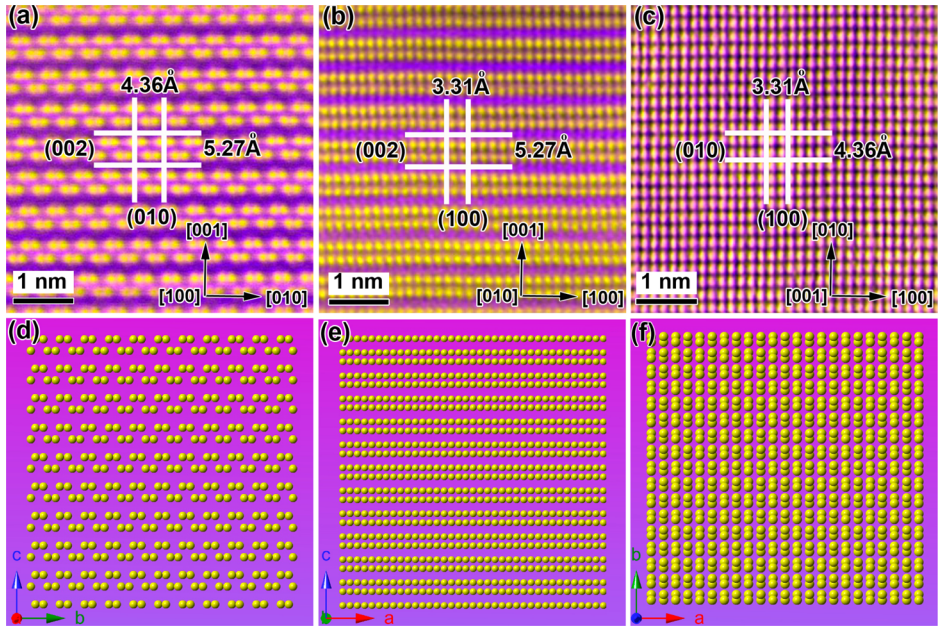

Figure 2. Atomic-scale STEM-HAADF images of bulk BP at different zone axes. (a–c) Atomic HAADF images of pristine bulk BP taken at the [100], [010], and [001] zone axes, respectively. (d–f) Atomic models of well-known bulk BP projected along the *a*, *b*, and *c* directions, respectively.

DOI: 10.1021/acs.chemmater.6b05052
Chem. Mater. 2017, 29, 1350–1356

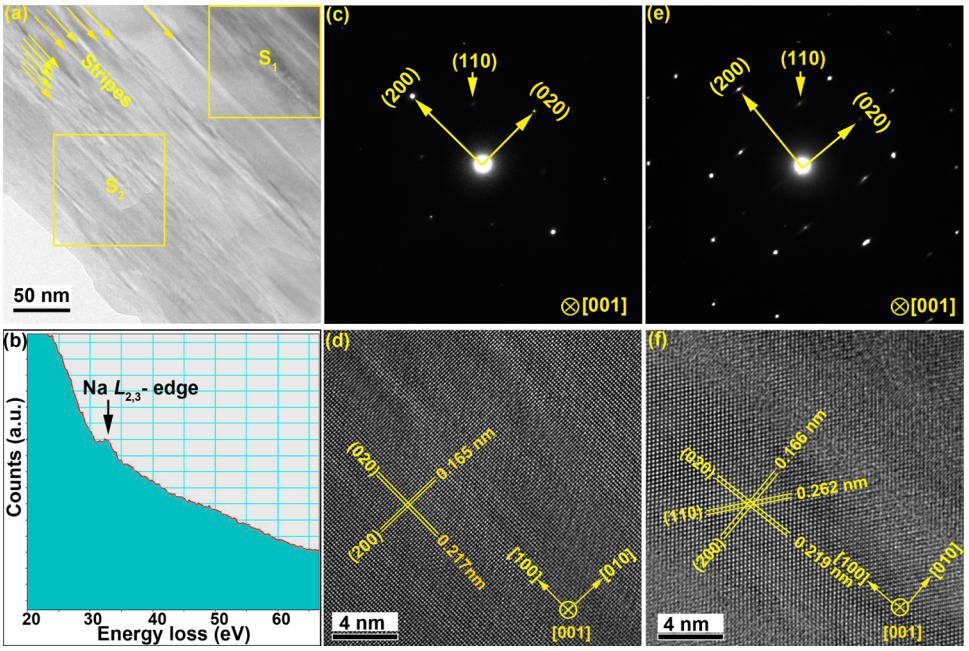

Figure 3. Structural evolution of partially sodiated BP. (a) Typical TEM image of the partially sodiated BP showing sodiation stripes. (b) EELS spectrum of the partially sodiated BP. The Na $L_{2,3}$ edge (31 eV) is captured in the area with high number of stripes. (c) SAED pattern taken from the area marked as S_1 in (a) at the [001] zone axis of the BP. (d) HRTEM image taken from area S_1 at the [001] zone axis of the BP. (e) SAED pattern taken from the area marked as S_2 in (a) at the [001] zone axis of the BP. (f) HRTEM image taken from area S_2 at the [001] zone axis of the BP.

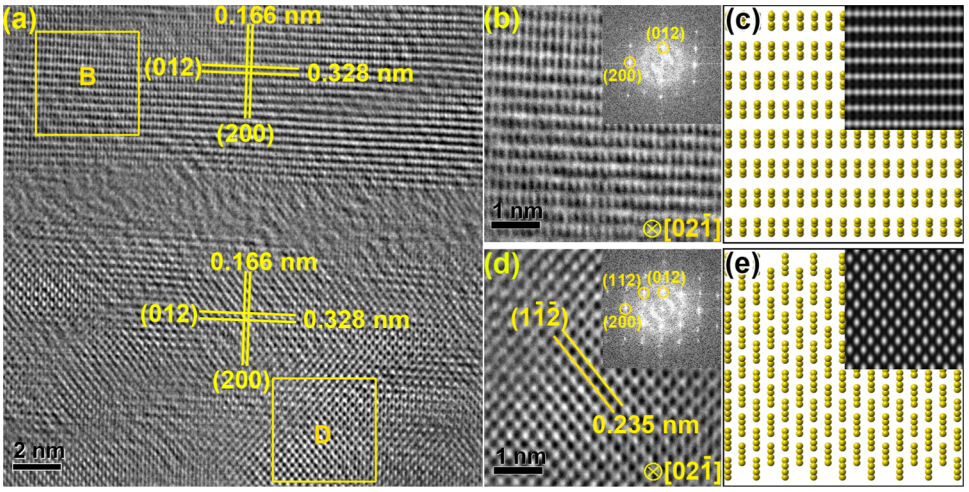

Figure 4. Atomic observation of partially sodiated BP with the [02$\bar{1}$] zone axis. (a) HRTEM image of partially sodiated BP at the [02$\bar{1}$] zone axis. Two domains with different atomic patterns are separated by a stripe. (b) HRTEM image taken from domain B marked in (a). The inset image is the corresponding FFT. (c) Atomic model of AB-stacked BP viewed at the [02$\bar{1}$] direction. The inset image is the corresponding simulated HRTEM image. (d) HRTEM image taken from domain D marked in (a). The inset image is the corresponding FFT. (e) Atomic model of AC-stacked BP viewed at the [02$\bar{1}$] direction. The inset image is the corresponding simulated HRTEM image.

Figure 3d shows an HRTEM image taken from domain S_1 at the [001] zone axis. An orthogonal atomic pattern similar to that in Figure 2c is clearly presented by this HRTEM image. The *d* spacings of different lattice planes were measured to be 0.217 and 0.165 nm, matching well with those of the (020) and (200) planes in AB-stacked BP. Figure 3e shows another SAED pattern taken from the domain marked S_2 containing many stripes. The intensity of the {110} spots is relatively higher than that of the {020} spots in the SAED pattern in Figure 3e. In addition, the diffraction spots in Figure 3e are stretched along the [010] direction. This indicates that the lattice in domain S_2 was distorted as a result of the penetration of the sodiation stripes. Figure 3f shows an HRTEM image taken from domain S_2 at the same zone axis. Interestingly, we found that the HRTEM in Figure 3f exhibited a hexagonal-like atomic arrangement, which differs greatly from that in Figure 3d. The (020) and (200) lattice planes in Figure 3f show *d* spacings of 0.219 and 0.166 nm, respectively, which are similar to those in Figure 3d, while a well-defined (110) lattice plane with a *d* spacing of 0.262 nm stands out in Figure 3f. The atomic arrangement in the lattice of Figure 3f is very close to that of AA- or AC-stacked BP viewed in the *c* direction (Figure 1a,c). In addition, stripes parallel to the (020) planes at the [100] directions are clearly shown in Figure 3f. The lattice in the stripes shows an amorphous feature, which corresponds well to the stretched spots in the SAED pattern in Figure 3e. Through

DOI: 10.1021/acs.chemmater.6b05052
Chem. Mater. 2017, 29, 1350−1356

the above analysis, we note that a lattice reordering was driven by the sodiation of BP and that the newly formed BP has the AA or AC stacking sequence. However, it is difficult to differentiate the exact stacking order using only the HRTEM image taken along the [001] direction because the AA and AC stacking orders in BP have the same atomic patterns when viewed along the *c* direction.

To identify the newly observed layering order, we examined the partially sodiated BP from other zone axes. Figure 4a shows an HRTEM image of the partially sodiated BP indicating two domains with different phases. The measured *d* spacings of the crossed lattice planes in the HRTEM image are 0.166 and 0.328 nm, which are highly consistent with those of the (200) and (012) lattice planes of BP, respectively. Correspondingly, the HRTEM image shown in Figure 4a is also determined to be taken at the $[02\bar{1}]$ zone axis. An enlarged HRTEM image from domain B marked in Figure 4a is shown in Figure 4b, where we clearly see an orthogonal atomic pattern. The corresponding fast Fourier transform (FFT) pattern is also displayed in the inset of Figure 4b, and the spots for the (200) and (012) planes are indicated. The atomic arrangement in domain D perfectly matches the well-known atomic model of AB-stacked BP projected in the $[02\bar{1}]$ direction, as shown in Figure 4c. The simulated HRTEM image based on this atomic model was also constructed and is shown in the inset of Figure 4c. The above analysis indicates that the lattice in domain D belongs to AB-stacked BP at the $[02\bar{1}]$ zone axis. Figure 4d shows an enlarged HRTEM image from domain D, where we observe a different atomic arrangement from that in Figure 4b. Obviously, a well-defined $(1\bar{1}2)$ lattice plane with a *d* spacing of 0.235 nm has appeared in Figure 4d. The corresponding FFT in the inset of Figure 4d also clearly exhibits the {112} spots. The atomic model of AC-stacked BP with the $[02\bar{1}]$ projection is shown in Figure 4e. We can see that the atomic arrangement pattern of Figure 4d is very close to this model. The corresponding simulated HRTEM at the inset of Figure 4e also indicates that the lattice in the domain D belongs to AC-stacked BP rather than AA-stacked BP (see the supporting model of AA-stacked BP with the same zone axis in Figure S1).

To better explain the experimental observations, we conducted density functional theory (DFT) simulations to capture the effect of sodium intercalation on the structure of bulk BP while considering the van der Waals corrections. It has been demonstrated that van der Waals interactions play an important role in the structure and elastic properties of BP.[18−20] Therefore, it is very important to check the structure of the ground state of BP by using different van der Waals corrections. In this work, the effects of dispersion forces were addressed by means of the vdW-DF1,[21] vdW-DF2,[22] and semiempirical DFT-D functionals.[23,24] Table 1 lists the lattice constants of BP from experiment[25] and from simulations using different van der Waals corrections. For the in-plane lattice constants (*a* and *b*), there is only a slight difference in using functionals with various van der Waals corrections, such as DFT-D, vdW-DF1, and vdW-DF2. Also, the in-plane lattice constants are in good agreement with the previous reports.[18,20] One can find that van der Waals interactions have a significant effect on the lattice constant *c*, and the DFT-D method is the best correction method to reproduce the experimental lattice constant *c*. Therefore, the DFT-D method was chosen as the approximation to describe van der Waals interactions between layers in BP in the present work. The binding energy for layered compounds can be used to evaluate the layer−layer interactions. Here we define the binding energy for bulk BP as $(2 \times E_{\text{monolayer}} - E_{\text{bulk}})/(2 \times \text{area})$. The binding energies for graphite, BP, and MoS_2 are 13.37, 14.81, and 15.89 meV/Å^2, respectively. The experimental results show that Li ions can intercalate into graphite and MoS_2.[10,26] Thus, one can expect that alkali ions such as Li and Na could also intercalate into bulk BP.

Table 1. Lattice Constants of Bulk BP from the Experiment in Ref 25 and Our Simulations Using Different van der Waals Correction Approximations

	a (Å)	*b* (Å)	*c* (Å)
experiment	3.32	4.39	10.52
PBE	3.31	4.61	13.21
vdw-DF	3.35	4.71	11.92
vdw-DF2	3.39	4.76	11.74
DFT-D	3.32	4.46	10.92

The unit cell model of bulk BP contains bilayer phosphorene with the AB stacking order. Movies S1 and S2 show the energy, volume, and structure evolution for bulk BP with one- and two-layer sodium intercalation in the structure relaxation process, respectively. Figure 5a,b shows the total energy and volume evolution, respectively, of bulk BP with two-layer sodium intercalation in the structural relaxation process. During the atomic relaxation process, the energy of the system decreases and the volume of the system fluctuates and then stabilizes. After relaxation, the BP with sodium intercalation is transformed into another orthorhombic structure with space group *Imm*2 (No. 44). The side views of the initial and relaxed structures are shown in Figure 5c,d, respectively. Sodium intercalation causes changes in the BP lattice constants. For sodium-intercalated BP with a concentration of about 25%, the lattice constants for the structure are $a = 3.28$ Å, $b = 4.58$ Å, and $c = 13.18$ Å. By comparing with pristine BP, we conclude that after sodiation the lattice parameter *a* shrinks while *b* and *c* expand. More importantly, we notice that BP expands about 20.70% along the *c* direction. Here we confirmed the presence of the AC stacking in BP after sodium intercalation by simulation.

In the above discussion, we have experimentally and theoretically demonstrated the transition from AB to AC in the initial sodiation process. By transitioning from AB to AC stacking order, the intercalated region can reduce its energy (total energy). On the other hand, the pristine regions prefer to keep the AB stacking order. If the energy that can be released from the reordering in the intercalated region is less than the increased energy in the pristine regions, the energy of whole system will increase, and the stacking reordering can not happen. With increasing concentration of sodium in the intercalated region, if the intercalated region is confined by the pristine AB stacking lattice, its lattice structure will be destroyed and change into an amorphous structure. This is the origin of the lattice constraint. In the initial sodiation stage, most regions without sodium intercalation still keep AB stacking order, which hinders the AB-to-AC reordering of the local region with sodium intercalation. We have noted that there are atomic disordered regions formed in bulk BP after sodiation. We believe that the disordering of stripes is attributed to the constraint of the BP lattice. Figure 6a−d shows one, two, four, and six sodium atoms intercalated in trilayer BP after relaxation, respectively. In the relaxation

DOI: 10.1021/acs.chemmater.6b05052
Chem. Mater. 2017, 29, 1350−1356

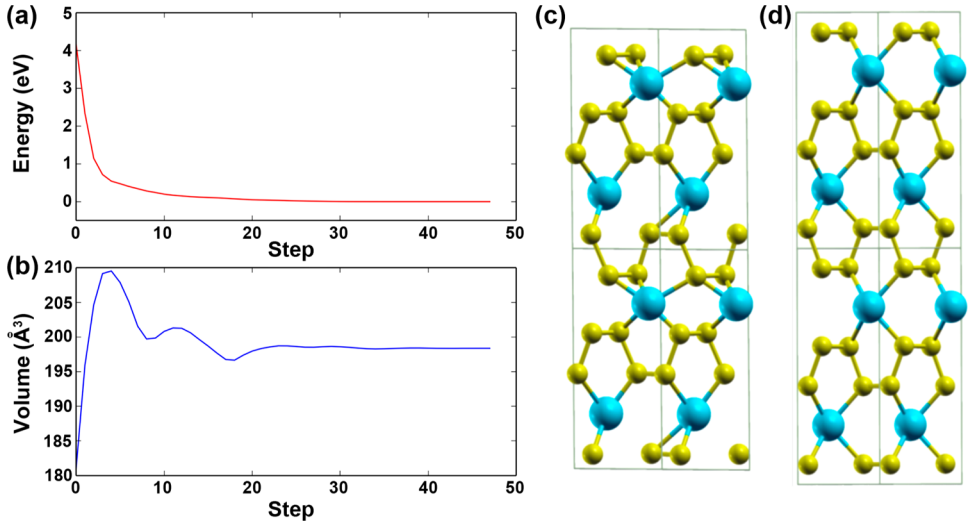

Figure 5. Relaxation of bulk black phosphorus with sodium intercalation. (a) Energy and (b) volume changes of bulk black phosphorus as functions of the number of relaxation steps. (c, d) Atomic models of (c) initial and (d) relaxed black phosphorus structures with sodium intercalation, respectively. Yellow balls represent phosphorus atoms, and blue balls represent sodium atoms.

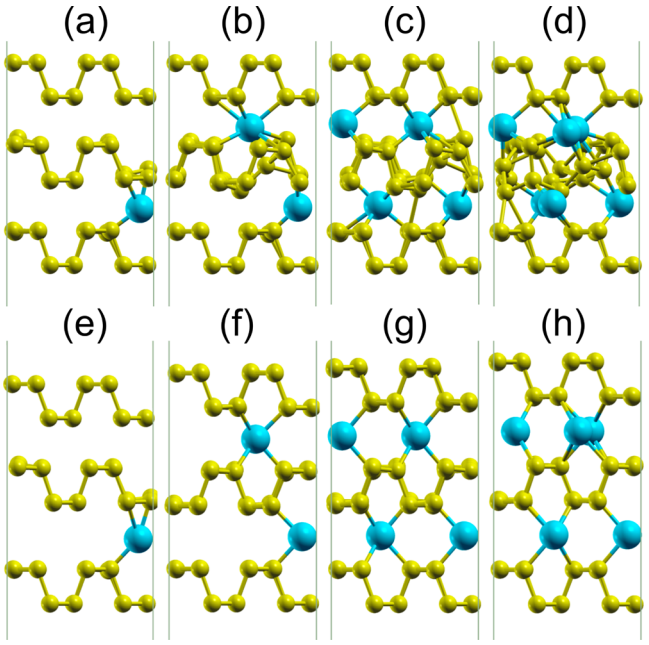

Figure 6. Structural evolution of trilayer phosphorene with different sodium concentrations. (a–d) Trilayer phosphorene with (a) one, (b) two, (c) four, and (d) six sodium atoms intercalated in the middle layer with the phosphorus atoms in the bottom and top planes fixed. (e–h) Trilayer phosphorene with (e) one, (f) two, (g) four, and (h) six sodium atoms intercalated in the middle layer without the phosphorus atoms fixed. Yellow balls represent phosphorus atoms, and blue balls represent sodium atoms.

process, we maintained the layer–layer distance and fixed the top and bottom layers of phosphorus. It is very clear that the structure of the multilayer BP has been distorted with the addition of sodium atoms and that the distortion is correlated to the intercalated ion concentration. The more sodium atoms are intercalated, the more distortion in the middle layer is observed (Figure 6a–d). This can explain the formation of the disordered stripes observed in our experiments. Upon a further increase in the intercalated sodium concentration, the P–P bonds in the same layer weaken and finally break. It should be noted that after amorphization the layered structure is unrecoverable.

The amorphization of the lattice releases the constraint. Therefore, we also calculated the structure of the sodium-intercalated trilayer BP. Figure 6e–h shows atomic structures of trilayer BP with different sodium concentrations without the lattice constraint. We can observe that the BP layers transform to AC stacking order. In addition, we find that if there is no sodium between the two adjacent layers the two layers still keep the AB ordering, as shown in Figure 6e. As we mentioned before, there is about 20% expansion along the *c* direction for bulk BP with 25% sodium concentration.

Bulk BP is direct semiconductor with a band gap of 0.3 eV.[12] Though DFT-D corrections can reproduce the lattice constants for the layered compound very well, they cannot precisely describe its electronic properties because of the correlation's empirical nature.[27] Figure S2a–d shows the band structures for bulk BP obtained using the PBE functional and the corrected functionals DFT-D, vdw-DF1, and vdw-DF2, respectively. Figure S2a shows a band gap of 0.1 eV obtained using the PBE functional without van der Waals interaction corrections, which is underestimated because of the overestimated lattice parameter *c* and the well-known problem of DFT in predicting the band gap. The band structure of bulk BP shows a metallic nature if the DFT-D functional with corrections is employed (Figure S2b). However, vdw-DF1 and vdw-DF2 can give an acceptable band gap of 0.4 eV for bulk BP (Figure S2c,d). Therefore, the vdw-DF2 correction was used for electronic properties calculations.

Because the as-grown BP is always p-type, sodium intercalation can be used as a method to make electrons be the carriers, which has a great impact on p–n junction fabrication. For bulk BP with a sodium concentration of 12.5%, the structure with AC stacking order is the most stable one. The band structure shown in Figure S3 indicates its metallic nature, and the partial density of states shows that the Na 3s and P 2p orbitals are hybridized and both contribute to the conductivity.

We checked other alkali or metal intercalation systems and found that most foreign atoms can induce stacking reordering, such as Li, K, Ca, and Cu (see Figure S4). The shift of adjacent

DOI: 10.1021/acs.chemmater.6b05052
Chem. Mater. 2017, 29, 1350–1356

layers depends on the type of intercalated atom. For example, the shift of adjacent layers induced by K and Ca are greater than those induced by Li and Cu because of the atomic radius difference. In addition, intercalation of foreign metal atoms can also induce n-type doping in BP. We have demonstrated that sodiated BP is n-type-doped by simulation. Recently, it was also experimentally demonstrated that the addition of Cu atoms can induce n-type doping without degrading the transport properties of BP.[28] The major carrier for most BP is holes, and therefore, n-type BP is desired for electronic applications, such as FETs and complementary metal−oxide−semiconductor (CMOS). The crystalline structure of BP should be maintained to keep the high mobility of carriers during the electron introduction process. The intercalation of metal atoms can keep the crystalline structure and introduce n-type carriers, which suggests that the metal intercalation methodology would be a promising strategy for carrier modification. In the present work, we experimentally demonstrated not only that stacking reordering is induced by sodium intercalation, and we have predicted that most metal atoms should have a similar effect. Experimental verification of the effects of intercalating other metals is needed.

CONCLUSIONS

Using DFT simulations and in situ TEM techniques, we studied the atomistic structural evolution in black phosphorus under sodium intercalation. Our results show a two-stage sodiation mechanism in black phosphorus. Upon sodium intercalation, the stacking order of black phosphorus changes from AB to AC. Subsequently, we observed amorphous stripes formed in BP during the sodiation process. This phenomenon was attributed to the lattice constraint of BP. The intercalation of sodium or other metals not only induces structural evolution but also modulates the electronic structure, such as the carrier type. This suggests new opportunities to exploit alloyed BP for nanoelectronic applications.

EXPERIMENTAL SECTION

Sample Preparation. A 0.1 mg sample of bulk BP (purchased from Smart Elements) was ground with a mortar and pestle and then immersed in 20 mL of isopropyl alcohol (IPA). The sample was sonicated in a Sonics Vibra-Cell sonicator (130 W) for 5 h and then kept still for 20 min. The supernatant was used in this experiment.

In Situ Experiments. The BP sample was attached to a gold wire to build an in situ sodium ion cell inside the transmission electron microscope. The gold wire also acted as a current collector on the nanoflake side. Sodium metal, which served as the counter electrode, was scratched using a tungsten wire inside the glovebox filled with Ar. The two electrodes were mounted onto a biasing-TEM sample holder (Nanofactory Instruments), which was transferred in an airtight container and loaded into the TEM column. The naturally grown Na_2O and NaOH layer on the surface of the sodium metal served as the solid electrolyte for Na transport. The (Na_2O + NaOH)/Na electrode side was moved forward to contact one of BP nanoflakes. Once a reliable electrical contact was built, potential of −0.5 V was applied to the phosphorene flake to initiate the sodiation. The sodiation experiments were carried out inside an aberration-corrected JEOL JEM-ARM200CF scanning transmission electron microscope operated at 80 kV. The HAADF images were acquired using a 22 mrad probe convergence angle and a 90−370 mrad collection angle. The EELS spectra were obtained with a 45 mrad collection angle. HRTEM simulations were carried out using the multislice method implemented in the QSTEM code, which uses Dirac−Fock ionic scattering potentials provided by David Rez, Peter Rez, and Ian Grant. The parameters for HRTEM simulations include an accelerating voltage of 200 kV, a convergence angle of 0.2 mrad, 1.2 mm Cs, and a focal spread of 4 nm.

Simulation. All of the calculations were conducted using the Quantum-ESPRESSO package[29] in the DFT framework. We employed ultrasoft pseudopotentials[30] as well as the generalized gradient approximation in the Perdew−Burke−Ernzerhof (PBE) parametrization[31] of the exchange−correlation functional. A self-consistent energy accuracy of 1.4×10^{-9} eV, residual forces below 2.6×10^{-3} eV/Å, and a total energy convergence of 1.4×10^{-4} eV were achieved. Because of the layered structure of BP, the interactions between layers are van der Waals interactions. While DFT provides a many-particle framework that in principle incorporates both local and nonlocal interactions, the standard semilocal approximation used in DFT neglects the long-range attractive contribution (London dispersion forces). The effects of dispersion forces have been considered in our present study. We calculated the transition barriers for stacking reordering using the nudged elastic band method.[32−34] The concentration of alkali in BP can be defined as $C = (N_{Li/Na}/N_P) \times 100\%$.

ASSOCIATED CONTENT

Supporting Information

The Supporting Information is available free of charge on the ACS Publications website at DOI: 10.1021/acs.chemmater.6b05052.

Additional simulated data (PDF)

Energy, volume, and structure evolution for bulk BP with one-layer sodium intercalation in the structure relaxation process (AVI)

Energy, volume, and structure evolution for bulk BP with two-layer sodium intercalation in the structure relaxation process (AVI)

AUTHOR INFORMATION

Corresponding Authors

*E-mail: anmin@shu.edu.cn (A.N.).
*E-mail: iamwhuang@njtech.edu.cn (W.H.).
*E-mail: rsyassar@uic.edu (R.S.-Y.).
*E-mail: mashayek@uic.edu (F.M.).

ORCID

Yingchun Cheng: 0000-0002-8495-9184
Anmin Nie: 0000-0002-0180-1366
Wei Huang: 0000-0001-7004-6408
Reza Shahbazian-Yassar: 0000-0002-7744-4780

Notes

The authors declare no competing financial interest.

ACKNOWLEDGMENTS

This work was supported by the National Natural Science Foundation of China (11504169, 61575094, and 61136003), the National Basic Research Program of China (2015CB932200), and Synergetic Innovation Center for Organic Electronics and Information Displays. The research reported in this publication was supported by partial funding from King Abdullah University of Science and Technology (KAUST). R.S.-Y. acknowledges financial support from the U.S. National Science Foundation (Award CMMI-1619743). A.N. acknowledges support by the Shanghai Youth Talent Program and the Program for Professor of Special Appointment (Eastern Scholar) at Shanghai Institutions of Higher Learning. The acquisition of the UIC JEOL JEM-ARM200CF microscope was supported by an MRI-R2 Grant from the U.S. National Science Foundation (Award DMR-0959470).

DOI: 10.1021/acs.chemmater.6b05052
Chem. Mater. 2017, 29, 1350−1356

REFERENCES

(1) Li, L.; Yu, Y.; Ye, G. J.; Ge, Q.; Ou, X.; Wu, H.; Feng, D.; Chen, X. H.; Zhang, Y. Black phosphorus field-effect transistors. *Nat. Nanotechnol.* **2014**, *9*, 372−377.

(2) Tran, V.; Soklaski, R.; Liang, Y.; Yang, L. Layer-controlled band gap and anisotropic excitons in few-layer black phosphorus. *Phys. Rev. B: Condens. Matter Mater. Phys.* **2014**, *89*, 235319.

(3) Peng, X.; Wei, Q.; Copple, A. Strain-engineered direct-indirect band gap transition and its mechanism in two-dimensional phosphorene. *Phys. Rev. B: Condens. Matter Mater. Phys.* **2014**, *90*, 085402.

(4) Rodin, A. S.; Carvalho, A.; Castro Neto, A. H. Strain-induced gap modification in black phosphorus. *Phys. Rev. Lett.* **2014**, *112*, 176801.

(5) Kim, J.; Baik, S. S.; Ryu, S. H.; Sohn, Y.; Park, S.; Park, B.-G.; Denlinger, J.; Yi, Y.; Choi, H. J.; Kim, K. S. Observation of tunable band gap and anisotropic Dirac semimetal state in black phosphorus. *Science* **2015**, *349*, 723−726.

(6) Liu, H. J.; Jiao, L.; Xie, L.; Yang, F.; Chen, J. L.; Ho, W. K.; Gao, C. L.; Jia, J. F.; Cui, X. D.; Xie, M. H. Molecular-beam epitaxy of monolayer and bilayer WSe2: a scanning tunneling microscopy/spectroscopy study and deduction of exciton binding energy. *2D Mater.* **2015**, *2*, 034004.

(7) Cancado, L. G.; Takai, K.; Enoki, T.; Endo, M.; Kim, Y. A.; Mizusaki, H.; Speziali, N. L.; Jorio, A.; Pimenta, M. A. Measuring the degree of stacking order in graphite by Raman spectroscopy. *Carbon* **2008**, *46*, 272−275.

(8) Yan, J.; Xia, J.; Wang, X.; Liu, L.; Kuo, J. L.; Tay, B. K.; Chen, S.; Zhou, W.; Liu, Z.; Shen, Z. X. Stacking-Dependent Interlayer Coupling in Trilayer MoS2 with Broken Inversion Symmetry. *Nano Lett.* **2015**, *15*, 8155−8161.

(9) Zhu, Z. Y.; Cheng, Y. C.; Schwingenschlogl, U. Giant spin-orbit-induced spin splitting in two-dimensional transition-metal dichalcogenide semiconductors. *Phys. Rev. B: Condens. Matter Mater. Phys.* **2011**, *84*, 153402.

(10) Belash, I. T.; Bronnikov, A. D.; Zharikov, O. V.; Pal'nichenko, A. V. Superconductivity of Graphite-Intercalation Compound with Lithium C2li. *Solid State Commun.* **1989**, *69*, 921−923.

(11) Emery, N.; Herold, C.; d'Astuto, M.; Garcia, V.; Bellin, C.; Mareche, J. F.; Lagrange, P.; Loupias, G. Superconductivity of bulk CaC_6. *Phys. Rev. Lett.* **2005**, *95*, 087003.

(12) Dai, J.; Zeng, X. C. Bilayer Phosphorene: E ff ect of Stacking Order on Bandgap and Its Potential Applications in Thin-Film Solar Cells. *J. Phys. Chem. Lett.* **2014**, *5*, 1289−1293.

(13) Li, W.; Yang, Y.; Zhang, G.; Zhang, Y. W. Ultrafast and directional diffusion of lithium in phosphorene for high-performance lithium-ion battery. *Nano Lett.* **2015**, *15*, 1691−1697.

(14) Vishwanath, S.; Liu, X. Y.; Rouvimov, S.; Mende, P. C.; Azcatl, A.; McDonnell, S.; Wallace, R. M.; Feenstra, R. M.; Furdyna, J. K.; Jena, D.; Xing, H. G. Comprehensive structural and optical characterization of MBE grown $MoSe_2$ on graphite, CaF_2 and graphene. *2D Mater.* **2015**, *2*, 024007.

(15) Nie, A. M.; Cheng, Y. C.; Ning, S. C.; Foroozan, T.; Yasaei, P.; Li, W.; Song, B. A.; Yuan, Y. F.; Chen, L.; Salehi-Khojin, A.; Mashayek, F.; Shahbazian-Yassar, R. Selective Ionic Transport Pathways in Phosphorene. *Nano Lett.* **2016**, *16*, 2240−2247.

(16) Yu, X.-f.; Ushiyama, H.; Yamashita, K. Comparative Study of Sodium and Lithium Intercalation and Diffusion Mechanism in Black Phosphorus from First-principles Simulation. *Chem. Lett.* **2014**, *43*, 1940−1942.

(17) Huang, G. Q.; Xing, Z. W.; Xing, D. Y. Prediction of superconductivity in Li-intercalated bilayer phosphorene. *Appl. Phys. Lett.* **2015**, *106*, 113107−113107.

(18) Cai, Y.; Zhang, G.; Zhang, Y. W. Layer-dependent band alignment and work function of few-layer phosphorene. *Sci. Rep.* **2014**, *4*, 6677.

(19) Shulenburger, L.; Baczewski, A. D.; Zhu, Z.; Guan, J.; Tomanek, D. The Nature of the Interlayer Interaction in Bulk and Few-Layer Phosphorus. *Nano Lett.* **2015**, *15*, 8170−8175.

(20) Cai, Y.; Zhang, G.; Zhang, Y.-W. Electronic Properties of Phosphorene/Graphene and Phosphorene/Hexagonal Boron Nitride Heterostructures. *J. Phys. Chem. C* **2015**, *119*, 13929−13936.

(21) Dion, M.; Rydberg, H.; Schroder, E.; Langreth, D. C.; Lundqvist, B. I. van der Waals density functional for general geometries. *Phys. Rev. Lett.* **2004**, *92*, 246401.

(22) Lee, K.; Murray, E. D.; Kong, L. Z.; Lundqvist, B. I.; Langreth, D. C. Higher-accuracy van der Waals density functional. *Phys. Rev. B: Condens. Matter Mater. Phys.* **2010**, *82*, 081101.

(23) Grimme, S. Semiempirical GGA-type density functional constructed with a long-range dispersion correction. *J. Comput. Chem.* **2006**, *27*, 1787−1799.

(24) Appalakondaiah, S.; Vaitheeswaran, G.; Lebegue, S.; Christensen, N. E.; Svane, A. Effect of van der Waals interactions on the structural and elastic properties of black phosphorus. *Phys. Rev. B: Condens. Matter Mater. Phys.* **2012**, *86*, 035105.

(25) Hultgren, R.; Gingrich, N. S.; Warren, B. E. The Atomic Distribution in Red and Black Phosphorus and the Crystal Structure of Black Phosphorus. *J. Chem. Phys.* **1935**, *3*, 351−351.

(26) Cheng, Y. C.; Nie, A. M.; Zhang, Q. Y.; Gan, L. Y.; Shahbazian-Yassar, R.; Schwingenschlogl, U. Origin of the Phase Transition in Lithiated Molybdenum Disulfide. *ACS Nano* **2014**, *8*, 11447−11453.

(27) Cheng, Y. C.; Zhu, Z. Y.; Schwingenschlogl, U. Cl-intercalated graphene on SiC: Influence of van der Waals forces. *Europhys. Lett.* **2013**, *101*, 27008.

(28) Koenig, S. P.; Doganov, R. A.; Seixas, L.; Carvalho, A.; Tan, J. Y.; Watanabe, K.; Taniguchi, T.; Yakovlev, N.; Castro Neto, A. H.; Ozyilmaz, B. Electron Doping of Ultrathin Black Phosphorus with Cu Adatoms. *Nano Lett.* **2016**, *16*, 2145−2151.

(29) Giannozzi, P.; Baroni, S.; Bonini, N.; Calandra, M.; Car, R.; Cavazzoni, C.; Ceresoli, D.; Chiarotti, G. L.; Cococcioni, M.; Dabo, I.; Dal Corso, A.; de Gironcoli, S.; Fabris, S.; Fratesi, G.; Gebauer, R.; Gerstmann, U.; Gougoussis, C.; Kokalj, A.; Lazzeri, M.; Martin-Samos, L.; Marzari, N.; Mauri, F.; Mazzarello, R.; Paolini, S.; Pasquarello, A.; Paulatto, L.; Sbraccia, C.; Scandolo, S.; Sclauzero, G.; Seitsonen, A. P.; Smogunov, A.; Umari, P.; Wentzcovitch, R. M. QUANTUM ESPRESSO: a modular and open-source software project for quantum simulations of materials. *J. Phys.: Condens. Matter* **2009**, *21*, 395502.

(30) Vanderbilt, D. Soft Self-Consistent Pseudopotentials in a Generalized Eigenvalue Formalism. *Phys. Rev. B: Condens. Matter Mater. Phys.* **1990**, *41*, 7892.

(31) Perdew, J. P.; Burke, K.; Ernzerhof, M. Generalized Gradient Approximation Made Simple. *Phys. Rev. Lett.* **1996**, *77*, 3865−3868.

(32) Caspersen, K. J.; Carter, E. A. Finding transition states for crystalline solid-solid phase transformations. *Proc. Natl. Acad. Sci. U. S. A.* **2005**, *102*, 6738−6743.

(33) Henkelman, G.; Jonsson, H. A dimer method for finding saddle points on high dimensional potential surfaces using only first derivatives. *J. Chem. Phys.* **1999**, *111*, 7010−7022.

(34) E, W.; Ren, W. Q.; Vanden-Eijnden, E. String method for the study of rare events. *Phys. Rev. B: Condens. Matter Mater. Phys.* **2002**, *66*, 052301.

DOI: 10.1021/acs.chemmater.6b05052
Chem. Mater. 2017, 29, 1350−1356